Retinal Function and Structure in Ant1-Deficient Mice

M. Joseph Phillips,[1,2,3] *Sarah Webb-Wood,*[1] *Amanda E. Faulkner,*[1] *Seema B. Jabbar,*[1,2] *Valerie Biousse,*[2,4] *Nancy J. Newman,*[2,4] *Vi T. Do,*[2] *Jeffrey H. Boatright,*[2] *Douglas C. Wallace,*[5,6] *and Machelle T. Pardue*[1,2]

Purpose. Mutations in ANT, a mitochondrial ATP transporter, are typically associated with myopathy. Because of the high metabolic demands of the retina, the authors examined whether elimination of the *Ant1* isoform in a transgenic mouse affects retinal function or morphology.

Methods. RT-PCR was used to confirm *Ant1* expression in retinas of wild-type (WT) or *Ant1*$^{-/-}$ mice. Full-field ERGs were used to test retinal function under dark- and light-adapted conditions and the recovery of the photoresponse to a bright flash. Using histologic methods, the authors assessed the retinal location of ANT and ANT1-β-gal reporter protein, mitochondrial activity with cytochrome *c* oxidase (COX) and succinate dehydrogenase (SDH) staining, retinal layer thickness, and bipolar cell types using Chx10 and recoverin.

Results. *Ant1*$^{-/-}$ mice had supernormal ERG b-waves under both dark- and light-adapted conditions. X-Gal staining was detected in a subset of cells within the inner retina. The following characteristics were normal in *Ant1*$^{-/-}$ mice compared with age-matched WT mice: recovery of the photoresponse, COX and SDH activity, retinal morphology, and bipolar cell morphology.

Conclusions. The presence of ANT1 in a subset of inner retinal cells accompanied by supernormal ERG responses suggests that ANT1 may be localized to hyperpolarizing bipolar cells. However, the immunohistochemical techniques used here did not show any differences in bipolar cells. Moderate functional changes coupled with a lack of detectable morphologic changes suggest that ANT1 is not essential for ATP transport in the retina. (*Invest Ophthalmol Vis Sci.* 2010;51:6744–6752) DOI:10.1167/iovs.10-5421

From the [1]Rehabilitation Research and Development Center, Atlanta VA Medical Center, Decatur, Georgia; Departments of [2]Ophthalmology and [4]Neurology, and [5]Center for Molecular Medicine, Emory University, Atlanta, Georgia; and [6]ORU for Molecular and Mitochondrial Medicine and Genetics, University of California, Irvine, California.

[3]Present affiliation: University of Houston, College of Optometry, Houston, Texas.

Supported by the Rehabilitative Research and Development Service of the Department of Veterans Affairs, Research to Prevent Blindness, and National Institutes of Health Grants P30 EY06360, P30 AT000609, R01 EY014026, R01-NS41850 (DCW), and R01-NS21328 (DCW).

Submitted for publication February 22, 2010; revised May 31, 2010; accepted June 20, 2010.

Disclosure: **M.J. Phillips**, None; **S. Webb-Wood**, None; **A.E. Faulkner**, None; **S.B. Jabbar**, None; **V. Biousse**, None; **N.J. Newman**, None; **V.T. Do**, None; **J.H. Boatright**, None; **D.C. Wallace**, None; **M.T. Pardue**, None

Corresponding author: Machelle T. Pardue, Rehabilitation Research and Development Center, Atlanta VA Medical Center, 1670 Clairmont Road, Decatur, GA 30033; mpardue@emory.edu.

Mitochondrial metabolism is the primary source of aerobic energy generated by the transport of electrons into a chemiosmotic gradient across the inner membrane of the mitochondria. This complex process, called oxidative phosphorylation (OXPHOS), results in the production of adenosine triphosphate (ATP) within the mitochondria. ATP enters the cytosol through an exchange with ADP by way of adenine nucleotide translocator (ANT), which resides in the inner mitochondrial membrane.[1] ANT is expressed in mammals as four isoforms (ANT1, ANT2, ANT3, and ANT4) with varying degrees of tissue specificity.[2,3]

A transgenic mouse lacking *Ant1* has been generated that exhibits a loss of mitochondrial ATP.[4] As expected, this loss of ATP leads to mitochondrial proliferation in cardiac and skeletal muscle, as evidenced by increased histochemical staining for the mitochondrial enzymes cytochrome *c* oxidase (COX) and succinate dehydrogenase (SDH), and cardiac hypertrophy. In addition, the absence of *Ant1* inhibits OXPHOS, creating an increase in reactive oxygen species and mitochondrial DNA (mtDNA) mutations in the *Ant1*$^{-/-}$ mice with age.[5] Thus, the *Ant1*$^{-/-}$ mouse has been identified as a mouse model of mitochondrial myopathy and cardiomyopathy.[4]

The retina is one of the most metabolically active tissues in the body, with abundant mitochondria found in the photoreceptors and retinal pigment cells.[6] Given these high metabolic needs, retinal degeneration and visual deficits would seem likely when there is mitochondrial dysfunction. However, the most common ocular defect associated with mitochondrial myopathy is ophthalmoplegia, followed by optic neuropathy and pigmentary retinopathy,[7,8] all fairly rare diseases. Pigmentary retinopathy is most often seen in a subset of patients with chronic progressive external ophthalmoplegia, called Kearns-Sayre Syndrome, and in patients with MELAS (mitochondrial myopathy, encephalopathy, lactic acidosis, and stroke-like episodes) and MNGIE (mitochondrial neurogastrointestinal encephalomyopathy). Retinopathy in these conditions, though mainly involving the retinal pigment epithelium, is phenotypically variable and often subclinical.[9] Mutations in ANT1 are linked to autosomal dominant external ophthalmoplegia (adPEO).[10–13]

Our previous studies have shown *Ant1*$^{-/-}$ mice to be a pathologic model of adPEO.[14] The mice have been established as a model of mitochondrial myopathy and cardiomyopathy,[4] but retinal function and morphology have not been reported. To determine the role of ANT1 in the retina, retinal function and structure were examined in the *Ant1*$^{-/-}$ mouse.

Methods

Animals

Animal procedures conformed to the ARVO Statement for the Use of Animals in Ophthalmic and Vision Research and were approved by the local institutional animal care and use committee. *Ant1*$^{-/-}$ mice were raised on a 129SV background and obtained from a breeding colony

Investigative Ophthalmology & Visual Science, December 2010, Vol. 51, No. 12

established at Emory University. *Ant1*$^{-/-}$ mice were derived from transfected 129/Sv nuclei that were then mated to 129/Sv mice, creating a 129/Sv congenic line.[4] Mice were maintained through homozygous crossing with mutant and wild-type 129SV (WT) animals raised in the same room with similar environmental conditions and diet. To analyze the possible effects of age on the loss of *Ant1* in the retina, mice were tested within three age groups: 1 month old, 4 to 9 months old, and 18 to 24 months old.

A *β-geo* cassette containing both the LacZ and the neomycin resistance genes was inserted into the *Ant1* coding region,[4] creating *Ant1*$^{\beta\text{-geo}}$ mice. Detection of β-galactosidase activity by X-Gal staining was used as a marker for *Ant1* expression in these mice.

Reverse Transcription–Polymerase Chain Reaction

Retinal expression of *Ant1* mRNA in WT and *Ant1*$^{-/-}$ mice was assessed by reverse transcription–polymerase chain reaction (RT-PCR). Fresh retinal tissue was taken from 4- to 9-month-old and 18- to 24-month-old *Ant1*$^{-/-}$ mice and age-matched WT mice. The tissue was homogenized in the presence of RNA reaction reagents (RNAZol or RNABee; Tel-Test, Inc., Friendswood, TX), and RNA was extracted according to the manufacturer's instructions. RNA was amplified using a PCR system (SuperScript One Step RT-PCR System; Invitrogen, Carlsbad, CA) in accordance with the manufacturer's instructions. Reactions were conducted in an iQ detection system (iCycler; Bio-Rad Laboratories, Hercules, CA) with the following profile: 50°C for 30 minutes, 94°C for 2 minutes, followed by 40 cycles of 30 seconds each at 94°C, 57°C, and 72°C, and ending with 72°C for 10 minutes. Primers were designed to span introns based on comparing sequence data from GenBank entries of mouse mRNA (accession number U27315) and human genomic DNA (accession number AL683870), subsequently confirmed using the blastn algorithm in a BLAST2 search of a GenBank entry for mouse ANT1 coding sequence (accession number AF240002.1). Primers and other RT-PCR information are presented in Table 1. Reaction products were electrophoresed on a 5% polyacrylamide gel and visualized with ultraviolet light.

Electroretinography

Two experimental ERG protocols were followed. Mice for each protocol were dark adapted overnight and anesthetized with ketamine (80 mg/kg) and xylazine (16 mg/kg), and their eyes were dilated with 0.5% tropicamide and 0.5% cyclopentolate. ERGs were recorded using a stainless steel electrode loop resting on the corneal surface through a layer of 1% methylcellulose. Responses were referenced and grounded to needle electrodes placed in the cheek and tail, respectively. All stimuli were presented using a hand-held Ganzfeld controlled by a signal averaging system (Espion; Diagnosys, Littleton, MA), and responses were recorded from 0.03 to 1000 Hz.

Intensity Series Response. A standard dark- and light-adapted intensity series was recorded on *Ant1*$^{-/-}$ and age-matched WT mice to test rod and cone function in each age group. The dark-adapted stimuli consisted of eight flashes presented in increasing intensity from 0.001 to 10 cd · s/m^2. This was followed by a 10-minute light-adaptation period (20 cd/m^2) to saturate the rod response. Cone responses were isolated with the presentation of six flash stimuli at 2.1 Hz from 0.78 to 20 cd · s/m^2. Three to five responses were averaged for each dark-adapted flash intensity, and 25 responses were averaged for the light-adapted series.

Given that no differences were detected between the 1-month-old (n = 5/group) and 4- to 9-month-old (n = 9–10/group) animals, the ERG data were divided to represent young (1- to 9-month-old) and old (18- to 24-month-old; n = 10–11/group) mice. Statistical analysis between genotypes, ages, and flash intensities was performed with a two-way ANOVA (SigmaStat; Systat Software, Inc, San Jose, CA).

Photoreceptor Recovery Response. The second experimental ERG protocol was designed to test the recovery of the photoresponse to a bright flash in *Ant1*$^{-/-}$ mice from 18 to 24 months of age. This methodology had been used previously to show the ability of the visual cycle to regenerate the visual pigments needed to respond to a flash of light.[15] With a presumed lack of ATP in the *Ant1*$^{-/-}$ retina, this protocol enabled us to examine whether a loss of energy was causing a disruption in the recovery phase of the normal visual cycle. Older mice were used because evidence of an increase in reactive oxygen species production in the *Ant1*$^{-/-}$ mouse[5] would suggest the greatest insult to the mitochondria with age. After dark adaptation overnight, a standard flash (10 cd · s/m^2) was presented to elicit a "maximal" response. The eyes were then light adapted for 3 minutes using a 200 cd/m^2 background light. At the end of this adaptation period, the standard flash was presented every 100 seconds until the response recovered to the initial maximal "baseline" response or the animal awoke from anesthesia.

Histology and Immunohistochemistry

Light Microscopy Morphologic Analysis. After ERG testing, animals were killed and their eyes were enucleated. Eyes used to analyze general retinal morphology were immersion fixed in 2% paraformaldehyde/2.5% glutaraldehyde overnight and then rinsed in 0.1 M phosphate-buffered saline (PBS). After removal of the anterior portion of the eye, posterior eyecups were dehydrated in a graded alcohol series and embedded into resin (Embed 812/DER736; Electron Microscopy Sciences, Hatfield, PA). The eyecups were then sectioned on an ultramicrotome (Ultracut S; Reichert, Depew, NY) with thick sections (0.5 μm) stained with toluidine blue. Sections were viewed on a light microscope (DMB; Leica Microsystems, Bannockburn, IL) and digital images were captured (DC 300F; Leica Microsystems).

Table 1. Primers Used to Detect *Ant1* mRNA Expression

Primer	Sequence (5′→3′)	Nucleotide Position	Intron Spanned	Expected Product Size (nt)
Ant1A-S	TCCTGGCAGGTGGCATC	8243–8259	1	122
Ant1A-A	TTTGTACTGCTTCTCTGCACTG	9646–9667		
Ant1B-S	TGTCCAGGGCATCATCATCTACAG	10051–10074	2	167
Ant1B-A	GACGAACAGTGTCAAACGGATAGG	10677–10700		
Ant1-S	CAGGGCATCATCATCTACAGAGC	10055–10077	2	151
Ant1C-A	CAAACGGATAGGACACCAGCC	10668–10688		
Ant1D-S	GGCTGGTGTCCTATCCGTTTG	10668–10688	3, 4	133
Ant1D-A	GCGTTGGCTCCTTCATCTTTTG	11556–11577		

Four pairs of primers (Ant1A, Ant1B, Ant1C, Ant1D, with -S for sense and -A for antisense) were designed to span introns based on comparing sequence data from GenBank entries of mouse mRNA (accession number U27315) and human genomic DNA (accession number AL683870). Nucleotide position and intron information are based on GenBank accession number AF240002.1.

Anti-ANT Labeling. Eyes used for immunohistochemistry were immersion fixed in 4% paraformaldehyde for 30 minutes and then rinsed with 0.1 M PBS. The posterior eyecup was dissected from the rest of the eye and cryoprotected in 30% sucrose overnight. Eyecups were embedded in OCT medium and sectioned at 7 μm on a cryostat at −22°C. Sections were blocked (1.5% normal donkey serum) for 1 hour, followed by incubation overnight with the polyclonal anti-ANT (1:100; catalog number SC-9299; Santa Cruz Biotechnology, Inc., Santa Cruz, CA).[16] This antibody recognizes mouse ANT proteins, as demonstrated by Western blot and cell lysates (Santa Cruz Biotechnology, Inc. data sheet; http://www.scbt.com/datasheet-9299-ant-n-19.html). This polyclonal anti-ANT binds the *Ant1* isoform in skeletal muscle from $Ant1^{+/+}$ but not $Ant1^{-/-}$ mice.[17] After rinsing, sections were incubated for 30 minutes with the secondary antibody, 0.5% biotin-conjugated donkey anti-goat (Santa Cruz Biotechnology, Inc.). Sections were washed and then incubated for 30 minutes in the AB enzyme reagent (Santa Cruz Biotechnology, Inc.) and finally visualized using 3,3′-diaminobenzidine tetrahydrochloride (DAB). Sections were examined using bright-field microscopy (Leica DME; Leica Microsystems). Micrographs taken with a camera (Leica MPS 60; Leica Microsystems) using 35-mm slide film were digitized, and the intensity and pattern of labeling were subjectively compared.

COX and SDH Activity. To characterize mitochondrial function, COX and SDH and complex IV and II of the mitochondrial respiration chain, respectively, were histochemically assayed. Previously, studies have shown this technique to be successful in demonstrating mitochondrial enzyme activity in the retina.[18] Additional eyes were flash frozen in liquid nitrogen and cryosectioned at 7 μm to stain for COX and SDH enzyme activities, as previously described.[4] Sections were incubated at 37°C for 1 hour with COX (0.015 g COX, 1 mL catalase, 10 mg DAB, and 0.075 g sucrose in 0.2 M PBS) or SDH (2 M sodium succinate, 100 mg nitroblue tetrazolium, 0.05 M magnesium chloride [$MgCl_2$] in PBS). Sections were then washed and coverslipped (Crystalmount; Electron Microscopy Sciences). The presence of a brown or a blue product indicates COX or SDH enzyme activity, respectively.[4] All slides were examined using bright-field microscopy, and digital images were captured for comparison using a digital camera (Leica DME; Leica Microsystems). Images used for analysis were taken at the same intensity and exposure settings. Luminosity values were measured with digital imaging software (Photoshop; Adobe Systems Incorporated, San Jose, CA) for the background of each section (using the outer nuclear layer), the photoreceptor segments, and inner and outer plexiform layers. The relative difference from background was calculated (layer/background) and compared between $Ant1^{-/-}$ and WT retinas.

Detection of β-Galactosidase Activity by X-Gal Staining in $Ant1^{\beta\text{-geo}}$ Mouse Retina. Eyes from $Ant1^{\beta\text{-geo}}$ mice were immersion fixed in 0.5% glutaraldehyde for 1 hour, followed by a 1.5-hour LacZ rinse (0.01% sodium deoxycholate, 0.02% Nonidet-P40 and 2 mM $MgCl_2$ in 0.1 M PBS) and then cryoprotected in 30% sucrose overnight. Eyes were sectioned at 7 μm and postfixed in 0.5% glutaraldehyde for 5 minutes before being incubated overnight with X-Gal solution (5-bromo-4-chloro-3-indolyl β-D-galactopyranoside 40 mg/mL [Sigma-Aldrich, St. Louis, MO], 20 mM $K_3Fe(CN)_6$, 20 mM $K_4Fe(CN)_6$, 0.01% sodium deoxycholate, 0.02% Nonidet-P40, and 2 mM $MgCl_2$ in 0.1 M PBS] at room temperature. Sections were then washed, dehydrated, and coverslipped.

Bipolar Cell Labeling. Frozen sections, as prepared for anti-ANT labeling, were blocked (5% normal goat serum, 0.3% triton X-100) for 1 hour, followed by 2 days of incubation in anti-recoverin (1:1000; Millipore AB5585, Billerica, MA) or anti-Chx10 (1:1000; Abcam, Cambridge, MA). The sections were rinsed with 0.1 M PBS and incubated for 2 hours with AlexaFluor 488 secondary antibody (1:500; Molecular Probes, Carlsbad, CA). Sections were examined with a confocal microscope (Olympus, Center Valley, PA), and images were captured for qualitative analysis.

Results

Expression of *Ant1* in the Retina

Initial reports of $Ant1^{-/-}$ mice confirmed the presence of the *Ant1* isoform in the whole eye of WT mice.[4] To confirm that *Ant1* is expressed specifically in the retina and not just in the extraocular muscles that have been clinically implicated in *ANT1* mutations,[10] and to confirm that *Ant1* is not expressed in $Ant1^{-/-}$ mouse retinas, RT-PCR was performed on RNA isolated from retinas of WT and $Ant1^{-/-}$ mice. Figure 1 shows amplification products of RT-PCRs that used RNA from retinas of WT or $Ant1^{-/-}$ mice. Four primer pairs flanking introns 1, 2, or 3 and 4 of the mouse *Ant1* gene (GenBank accession number AF240002.1) were used. For all primer pairs, products of the correct length were obtained from WT retinal RNA. No RT-PCR products were obtained using $Ant1^{-/-}$ retinal RNA. These data indicate that *Ant1* is expressed in WT mouse retina but not in $Ant1^{-/-}$ mouse retina.

Retinal Function

Figure 2 illustrates a typical dark-adapted intensity series from young (1- to 9-month-old) and old (13- to 15-month-old) representative mice. Each graph shows representative responses from an $Ant1^{-/-}$ animal in the right column and an age-matched WT mouse in the left column. A typical ERG intensity series began with a dim flash from which a positive-going b-wave was elicited. As the flash intensity increased, the amplitude of the b-wave increased, and soon the b-wave was preceded by a negative a-wave. The a-wave is generated by the activity of the photoreceptors,[19,20] whereas the b-wave reflects bipolar cell activity.[21,22] As flash intensity increased further, the a-wave also increased in amplitude until the maximal response was elicited by the brightest flash presented. The leading edge of the b-wave contains small wavelets called oscillatory potentials (OPs) that are thought to be generated by the amacrine cells.[23,24] These OPs also became larger with flash intensity. These waveforms indicate that the $Ant1^{-/-}$ mice had larger amplitude a- and b-waves than did age-matched WT controls.

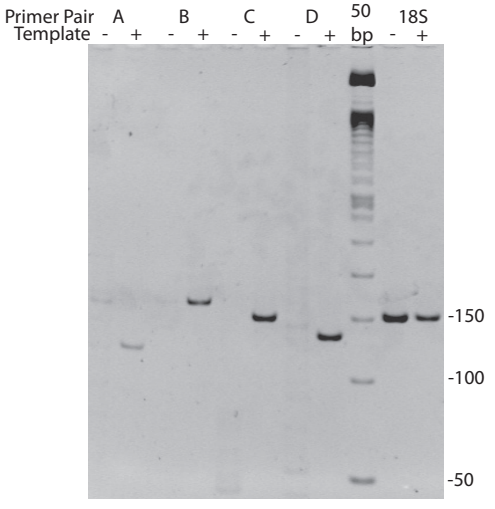

Figure 1. Image of polyacrylamide gel showing products from RT-PCR using whole RNA from retina as template and primer pairs designed to amplify four different regions of *Ant1* (see Table 1 for primer and amplicon details). RT-PCR products of correct size were obtained when using RNA from WT retinas as template (+). Conversely, products were not present when RNA from the $Ant1^{-/-}$ retina was used as a template (−), indicating the absence of *Ant1* mRNA in the retina.

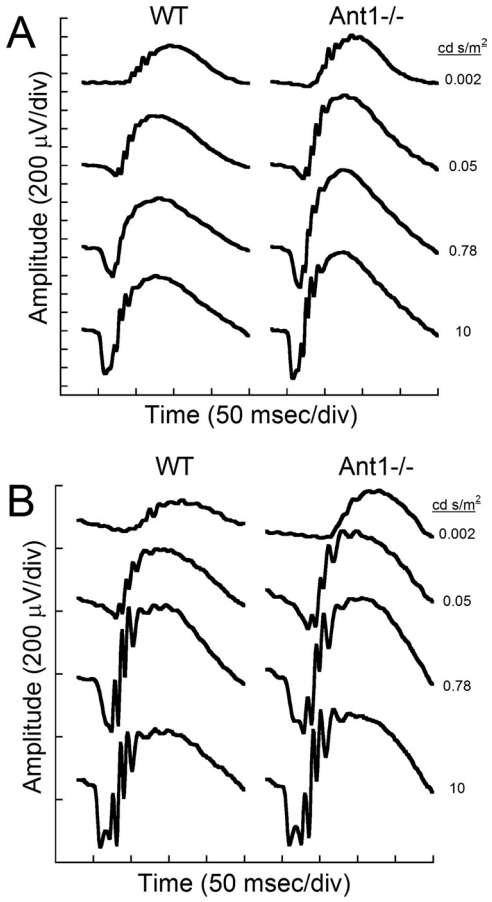

FIGURE 2. Representative ERG waveforms at increasing intensities from different *Ant1*$^{-/-}$ and WT mice at 4 to 9 months of age (**A**) and 13 to 25 months of age (**B**). Responses from the *Ant1*$^{-/-}$ mice are larger than from the age-matched WT mice.

Quantifications of ERG recordings are shown in Figure 3 as intensity-response curves for the a- and b-wave amplitudes. Figures 3A and 3B revealed an expected decrease in a- and b-wave amplitude with age in both genotypes, as previously reported.[25] Figure 3A shows the amplitude of the a-wave for young and old *Ant1*$^{-/-}$ and WT mice. There were no significant differences between *Ant1*$^{-/-}$ and WT mice from either age group.

Figure 3B shows the b-wave amplitudes for the two age groups. Overall, there was a significant increase in b-wave amplitude in the *Ant1*$^{-/-}$ mice compared with WT for young mice [$F(7,231) = 3.43$; $P = 0.002$] and old mice [$F(7,167) = 2.72$; $P = 0.0111$]. In young mice, the b-wave amplitude was approximately 16% larger in *Ant1*$^{-/-}$ than in WT mice. This supernormal response became a 27% increase in amplitude in the old *Ant1*$^{-/-}$ mice compared with age-matched WT mice.

To determine whether photoreceptor kinetics were affected by the *Ant1* mutation, the a-wave was normalized in *Ant1*$^{-/-}$ mice and WT controls from 4 to 9 months of age.[26,27] As shown in Figure 3C, the leading edge of the a-wave was the same for both groups of mice, suggesting similar phototransduction kinetics.

To determine whether the *Ant1*$^{-/-}$ retina recovered normally from a flash of light, mice were tested in a recovery paradigm in which a briefly light-adapted retina was probed with a standard flash until the response amplitude reached a predefined baseline. Figure 3D shows that the ability of the retina to recover from a short-duration light adaptation was similar for *Ant1*$^{-/-}$ and WT mice at 18 to 24 months of age.

To isolate cone responses, ERG recordings were made after saturating the rods with a background light. Responses recorded under these light-adapted conditions showed a trend for higher amplitudes in the *Ant1*$^{-/-}$ mice (Fig. 3E); however, the difference did not reach statistical significance. The light-adapted b-wave was 20% and 18% larger in young and old *Ant1*$^{-/-}$ mice, respectively, compared with age-matched WT controls. These data suggest that both rod- and cone-driven responses were affected by the absence of ANT1 in the retina.

For both the dark- and light-adapted responses, the implicit times between the *Ant1*$^{-/-}$ mice and age-matched WT mice were similar, with no indications of a delay or shortening in response (data not shown).

Retinal Structure

Figures 4A and 4B show normal retinal morphology of *Ant1*$^{-/-}$ and age-matched WT mice at 18 months of age. There were no indications of photoreceptor degeneration or other cell loss within the retinal layers of mutant mice. Measurement of retinal layer thickness (Table 2) in the *Ant1*$^{-/-}$ mice was similar to that found in WT mice with no statistically significant differences.

Expression and Location of ANT in the Retina

Localization of ANT in the Retina. To confirm the presence of ANT protein in the retina, retinas of WT mice were labeled with a polyclonal antibody for ANT that labels all isoforms of ANT. Figure 4C shows the labeling of all ANT isoforms in the WT retina with labeling in the inner segments, outer plexiform layer (OPL), inner nuclear layer (INL), inner plexiform layer (IPL), and ganglion cell layer (GCL). Because ANT is associated with mitochondria, the labeling of ANT isoforms in all retinal layers was expected, reflecting the high metabolic activity of the retina. Figure 4D shows ANT labeling in the *Ant1*$^{-/-}$ retina was also abundant, suggesting that the other isoforms of ANT were present. There was no detectable loss of polyclonal ANT antibody labeling in the *Ant1*$^{-/-}$ mice in any of the retinal layers.

***Ant1*$^{\beta\text{-geo}}$ Expression.** To specifically identify the expression and localization of ANT1 (as opposed to using a pan-ANT antibody, which recognizes all ANT isoforms) in the WT mouse retina, mice in which LacZ was inserted into the *Ant1* coding region were evaluated.[4] Retinal sections from *Ant1*$^{\beta\text{-geo}}$ mice showed punctate X-Gal staining in the OPL and IPL (Figs. 4E, 4F) at 4 months of age. Within the OPL, labeling was localized to the inner portion, whereas the labeling within the IPL transversed the entire layer with some puncta appearing in a vertical stack. Figure 4F shows a higher magnification image of the inner retina to illustrate the distinct spots and the localization of the staining in only the OPL and IPL.

OXPHOS Histochemistry in *Ant1*$^{-/-}$ Retinas

Fresh-frozen retinal sections of *Ant1*$^{-/-}$ retina exhibited both COX and SDH activity. In both *Ant1*$^{-/-}$ and WT retinas, COX activity resulting in brown labeling was seen in the inner segments and in the OPL and IPL (Figs. 5A, 5B). Given that *Ant1* expression was localized only to the OPL and IPL in the *Ant1*$^{\beta\text{-geo}}$ mice, these layers were more closely analyzed for potential differences in COX activity. In many of the WT retinas, punctate labeling could be identified in the OPL, whereas this was rarely seen in the *Ant1*$^{-/-}$ retinas. One possible explanation for this is that the *Ant1*$^{-/-}$ retinas have more intense COX activity that prevents these individual puncta from being visualized at the light microscopy level. However, no differences were detected between *Ant1*$^{-/-}$ mice and age-matched WT littermates when the intensity of the staining was quantified using histogram measurements (Table 3).

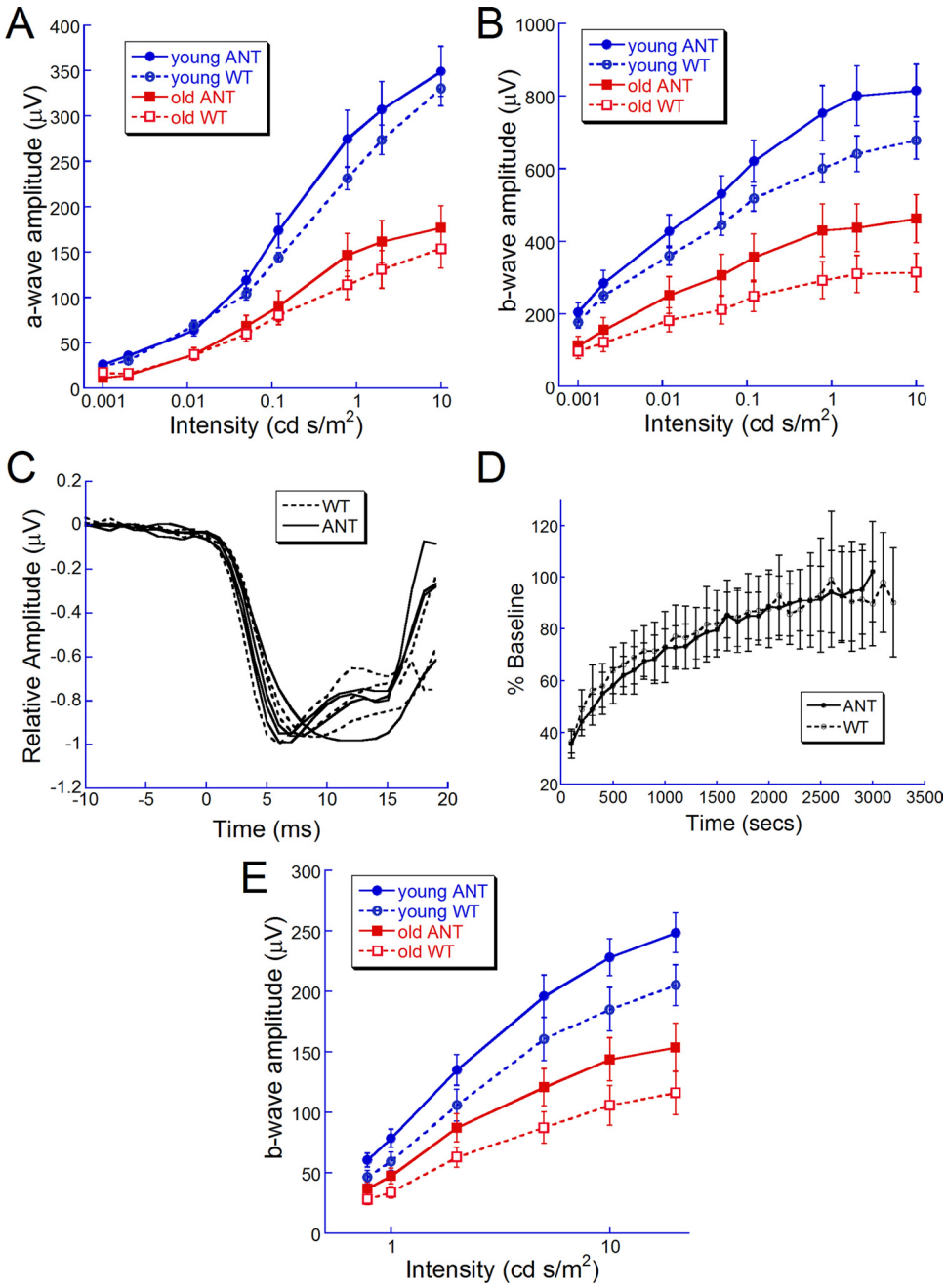

FIGURE 3. Intensity response function for young (1- to 9-month-old; n = 14–15/group) and old (13- to 25-month-old; n = 10–11/group) *Ant1*$^{-/-}$ and WT mice for the dark-adapted a-wave (**A**), dark-adapted b-wave (**B**), and light-adapted b-wave (**E**). The response from *Ant1*$^{-/-}$ mice was larger than that from WT for each ERG component and showed statistically significant increases for the dark-adapted b-wave (**B**; two-way ANOVA, young: $F(7, 231) = 3.43$, $P = 0.002$; old $F(7, 167) = 2.72$, $P = 0.0111$). No statistically significant differences were seen between genotypes for the a-wave (**A**) or light-adapted b-wave (**E**). (**C**) Plot of the normalized a-wave from *Ant1*$^{-/-}$ and WT mice. The kinetics of the response were similar for the two groups, indicating similar photoreceptor function. (**D**) Recovery response for *Ant1*$^{-/-}$ and WT mice. The *Ant1*$^{-/-}$ mice were able to recover normally from a bright flash of light.

SDH activity was observed in the inner and outer segments as well as the OPL and IPL. No differences in SDH activity were observed between the WT and *Ant1*$^{-/-}$ retinas (Figs. 5C, 5D; Table 3).

Bipolar Cell Morphology

To determine whether the hypernormal ERG response was caused by changes in the bipolar cell populations, we labeled WT and *Ant1*$^{-/-}$ retinas with a Chx10 antibody, which labels all types of bipolar cells,[28] and with a recoverin antibody, which labels only OFF or hyperpolarizing cone bipolar cells (HBC).[29] Figures 6A and 6B show that staining with the Chx10 antibody labeled a large population of nuclei in the INL. Anti-Chx10 labeling appeared similar between the WT (Fig. 6A) and *Ant1*$^{-/-}$ (Fig. 6B) retinas. Recoverin brightly labeled the ONL (not shown) and a subset of cells within the INL (Figs. 6C, 6D). The *Ant1*$^{-/-}$ retina clearly showed recoverin labeling in the INL, comparable to that seen in the WT retinas.

DISCUSSION

The data presented here suggest that some isoforms of ANT are abundant in the retina (Figs. 4C, 4D); however, the ANT1 isoform is primarily found only in the plexiform layers (Figs. 4E, 4F). Skeletal and cardiac muscles of the *Ant1*$^{-/-}$ mice show a loss of mitochondrial ATP and exercise intolerance[4]; we hypothesized a similar loss of ATP and subsequent loss of function would be seen within the retina. However, outer retinal function appears to be normal in the *Ant1*$^{-/-}$ mice because there was no significant difference in the a-wave amplitudes measured with the ERG. Inner retinal function was affected because the *Ant1*$^{-/-}$ mice exhibited supernormal

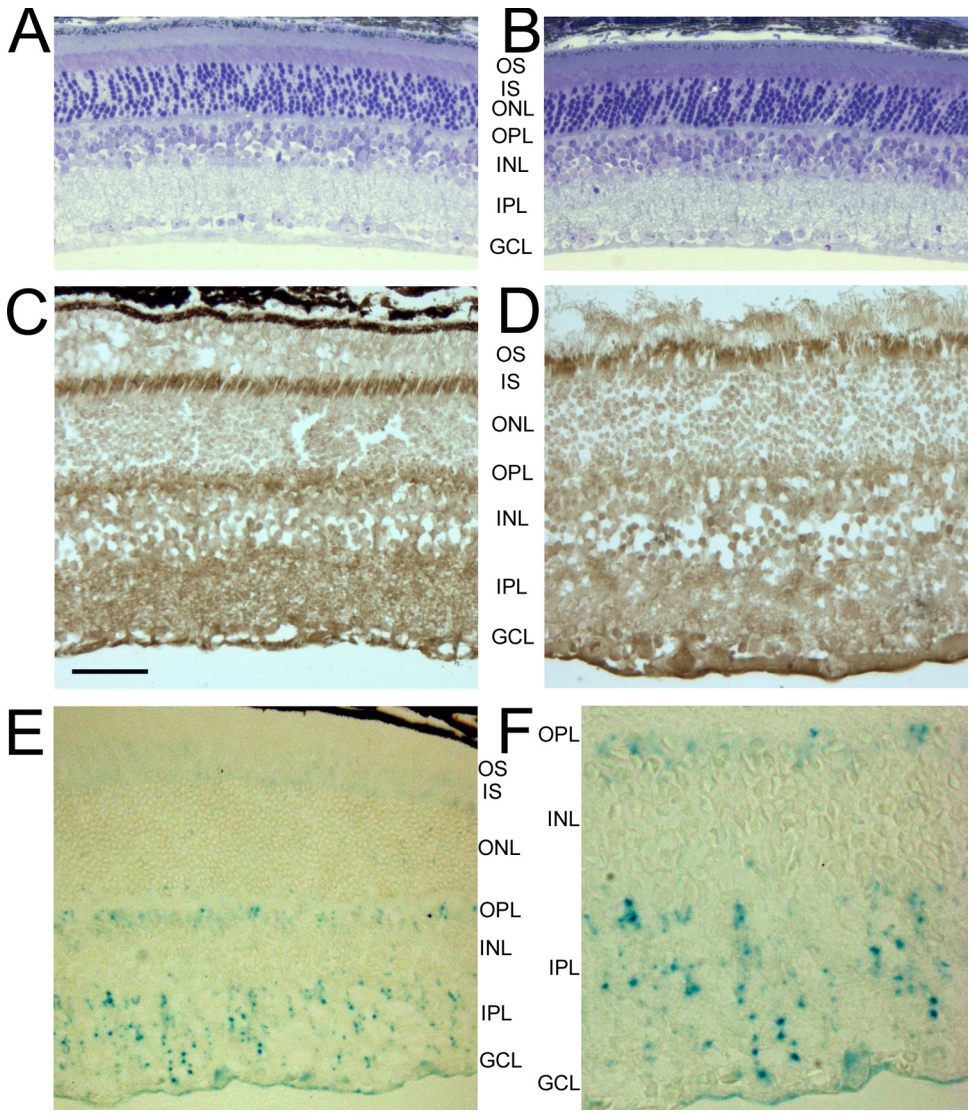

Figure 4. (**A**, **B**) Micrographs of toluidine blue–stained retinal sections from an age-matched WT mouse (**A**) and an *Ant1*$^{-/-}$ mouse (**B**) at 18 months of age. (**C**, **D**) Cryosections from 18-month-old *Ant1*$^{-/-}$ (**D**) and age-matched WT (**C**) retina showing anti-ANT labeling. This is a polyclonal antibody that labels all isoforms of ANT in the inner segments (IS), OPL, IPL, and GCL. (**E**) *Ant1*$^{\beta\text{-geo}}$ retina at 4 months of age stained with X-Gal to show the location of ANT1 in the retina. ANT1 punta are present in the outer and inner plexiform layers. (**F**) Higher magnification of (**E**) showing the X-Gal labeling in the inner retina. The pattern of staining suggests that ANT1 is localized to a subset of inner retinal cells. Scale bars: (**A**–**E**) 50 μm; (**F**) 35 μm. OS, outer segments.

ERG b-wave amplitudes (Figs. 2, 3). However, no dramatic morphologic changes in the inner retina were noted to account for the supernormal response.

Supernormal ERG Responses

The ERG is a summed response from a number of different retinal cells. The ERG a-wave is generated by the photoreceptors,[19,20] whereas the b-wave is generated primarily by the bipolar cells.[21,22] The major contribution to the b-wave is likely the ON or depolarizing bipolar cells (DBCs), which produce a large positive-going wave. The positive contribution to the b-wave was demonstrated nicely in pharmacologic experiments using 2-amino-4-phosphoonobutyric acid[30] or by mutant mice such as *nob*,[26] in which DBC activity was blocked, leaving only the negative-going a-wave derived from the photoreceptors. However, the HBC also contributed to this response as a negative wave that can be demonstrated by using *cis*-2,3-piperidine dicarboxylic acid and kynurenic acid to block their contribution, which results in a larger than normal b-wave.[31] Thus, one possible explanation for the supernormal responses in the *Ant1*$^{-/-}$ mice is that *Ant1* is specifically expressed in the HBCs, such that its loss in the *Ant1*$^{-/-}$ mouse would cause inactivity of these cells, thereby eliminating their negative input to the b-wave, and thus producing a larger b-wave response in *Ant1*$^{-/-}$ mice.

Table 2. Retinal Thickness Measurements from Age-Matched WT and *Ant1*$^{-/-}$ Mice

	+/+ (μm)	−/− (μm)
PR	58.59 ± 20.43	42.92 ± 8.32
ONL	73.58 ± 5.46	65.88 ± 10.78
OPL	10.08 ± 3.17	10.46 ± 2.34
INL	64.56 ± 2.69	64.38 ± 14.54
IPL	66.52 ± 12.77	75.83 ± 28.18
GCL	34.38 ± 5.12	35.29 ± 7.13

Ant1$^{-/-}$ retinas had normal layer thickness. PR, photoreceptors.

Similar abnormalities in inhibitory pathways have been implicated in clinically recorded supernormal ERG responses in patients with cone dystrophy.[32–34] Supernormal responses are relatively rare compared with the number of diminished responses seen in retinal disease. A comprehensive retrospective report on supernormal ERG responses by Heckenlively et al.[35] reported that maculopathy could be associated with responses greater than 2 SD above normal for photopic, scotopic, and bright flash stimuli. Because the macula is cone dense, this report could be interpreted as further support for the inhibi-

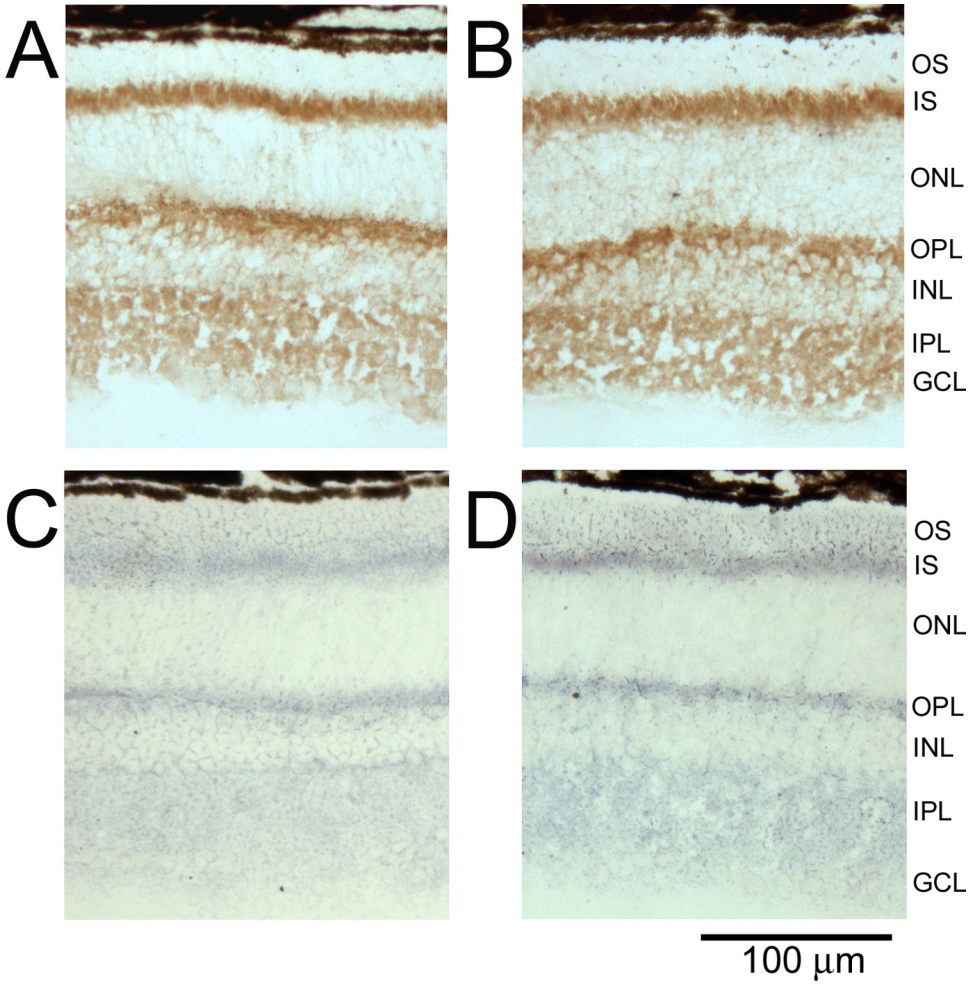

FIGURE 5. Representative COX (**A**, **B**) and SDH staining (**C**, **D**) of 4- to 9-month-old *Ant1*$^{-/-}$ and WT mice. COX and SDH labeling is clearly seen in the photoreceptor inner segments, OPL, and IPL of the WT (**A**, **C**) and *Ant1*$^{-/-}$ (**B**, **D**) retinas.

tory role of the hyperpolarizing cone pathway in the ERG response.

It has been reported that astrocytes of *Ant1*$^{-/-}$ mice have a decrease in glutamate uptake.[36] In the retina, glutamate is released in the darkness because of the flow of calcium through the photoreceptor ion channels. In the light, photoreceptor ion channels close, hyperpolarizing the photoreceptor and causing glutamate release to decrease. Thus, one consequence of the *Ant1* mutation in the retina may be an abundance of glutamate, resulting in more glutamate remaining in the synaptic cleft, which might lead to a more hyperpolarized state of the ON bipolar cells and a smaller b-wave. However, the *Ant1*$^{-/-}$ mice have supernormal b-wave responses. Furthermore, an excess of glutamate could lead to neuronal excitotoxicity and cell death; however, no significant differences were observed in individual layer thicknesses between WT and mutant retinas. Additionally, ATP has been implicated in synaptic transmission and the modulation of neurotransmitter release[37]; thus, the loss of ATP may produce a change in the kinetics of phototransduction. However, normalizing the leading edge of the a-wave in *Ant1*$^{-/-}$ mice (Fig. 3C) illustrated that the kinetics of the response were similar in affected and WT mice.

Another consequence of the lack of *Ant1* could be a chronic energy deficiency (as seen in the skeletal and cardiac muscle of Ant1$^{-/-}$ mice[4]) that decreases the mitochondrial ATP available for ion transport in retinal neurons. Decreased ATP could open ATP-sensitive potassium channels in retinal neurons,[38] which might simulate the dark-adapted state. However, in this scenario, it might be expected that the *Ant1*$^{-/-}$ retina would have a delay in the implicit time to a single flash or a delay in recovering from a flash of light because of the

TABLE 3. Ratio of Intensity between Each Layer Showing COX or SDH Activity Relative to the Background

	COX		SDH	
Layer	+/+	−/−	+/+	−/−
PR	0.61 ± 0.03	0.53 ± 0.05	0.81 ± 0.06	0.80 ± 0.08
OPL	0.70 ± 0.04	0.63 ± 0.07	0.85 ± 0.04	0.83 ± 0.08
IPL	0.77 ± 0.03	0.71 ± 0.05	0.90 ± 0.05	0.87 ± 0.06

Values are average ± SD. No significant differences were found between WT (+/+) and *Ant1*$^{-/-}$ retinas. PR, photoreceptors.

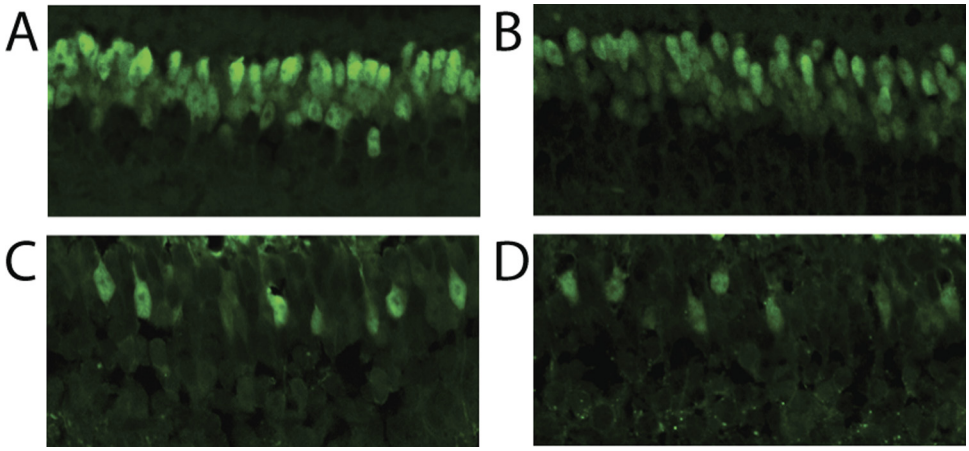

FIGURE 6. Chx10 (**A**, **B**) and recoverin (**C**, **D**) labeling of the INL in WT (**A**, **C**) and *Ant1*$^{-/-}$ mice (**B**, **D**). No differences were detected in the labeling patterns of WT and *Ant1*$^{-/-}$ mice.

increased flow of ions. No changes in implicit times or in recovery response (Fig. 3D) were seen between *Ant1*$^{-/-}$ and age-matched WT mice.

Alternatively, the larger b-wave amplitudes may be caused by an overcompensation of other ANT isoforms in the inner retinal cells to compensate for the loss of the ANT1 isoform. If ANT1 is present only in DBCs, then an abundance of ATP from the additional expression of ANT isoforms could make the DBCs super responders. However, if this hypothesis is correct, an increase in the level of COX and SDH staining might be expected in the plexiform layers, indicating increased OXPHOS activity. In fact, no qualitative or quantitative changes in COX and SDH staining were detected in the *Ant1*$^{-/-}$ retina (Fig 5; Table 3). Given that ANT1 is located in a subset of inner retinal cells, it is possible that COX and SDH are not sensitive enough at the light microscopy level to detect any changes. In addition, no upregulation of *Ant2* mRNA was detected in the brains of *Ant1*$^{-/-}$ mice, suggesting no compensation of the loss of the *Ant1* isoform in neural tissue.[4]

ANT1 Localization in the Retina

These results indicate that ANT isoforms, in general, are found abundantly in the murine retina (Figs. 4C, 4D). However, ANT1 appears to be expressed only in a subset of retinal cells, as indicated by the *Ant1*$^{\beta\text{-geo}}$ expression profile (Figs. 4E, 4F). Although is it unknown whether the beta galactosidase-linked ANT1 protein is trafficked as is native ANT1 in retinal cells, these results would seem to indicate only a small amount of ANT1 protein is present in the retina. Interestingly, ANT1 appeared to be present only in punctate locations in the IPL and OPL. In addition, the supernormal ERG b-wave may suggest an HBC localization, but no differences were detected in labeling between the ON and OFF sublaminae of the IPL to support this hypothesis.

Based on the supernormal ERG response, we hypothesized that ANT1 is located in either the HBCs or the DBCs. However, staining with a Chx10 antibody, which labels all bipolar cells,[28] or with a recoverin antibody, which labels HBCs,[29] did not show any gross abnormalities in *Ant1*$^{-/-}$ mice (Fig. 6). It is possible that the loss of ANT1 does not cause cell death; thus, immunostaining for Chx10 and recoverin would not reveal any change in the *Ant1*$^{-/-}$ retina. Future experiments could explore the possible cell types with colocalization experiments with antibodies specific for ANT1 to determine where ANT1 is located within the retina.

Mitochondrial Disease and Retinal Function

Although mitochondrial diseases can cause devastating phenotypes in muscles and heart, the retina is relatively spared. This is surprising considering the high energy demands of the retina.[39] Furthermore, approximately 90% of the retina's mitochondria are located in the photoreceptors,[40] presenting the possibility for drastic reductions in photoreceptor function with mitochondrial disorders. In a study of children with several mitochondrial disorders, Cooper et al.[41] found the majority of the patients to have abnormal scotopic responses, particularly delays in photoreceptor recovery. However, as in other studies of mitochondrial myopathy, the ERG abnormalities were relatively small and were not accompanied by clinical retinal degeneration.

In summary, we found that *Ant1*$^{-/-}$ mice, which have abnormalities of the extraocular muscles,[14] unexpectedly have normal retinal structure and *super*normal retinal function. The relative sparing of the retina in *Ant1*$^{-/-}$ mice may be explained by ANT1 localization to a subset of inner retinal cells. It may be that other ANT isoforms are more abundant in the retina or that there is a compensatory mechanism for the loss of a single isoform in this highly metabolic neural tissue.

Acknowledgments

The authors thank Tamara Barnett, Paulette Allard, and Kathy Knill for technical assistance and Alison Ziesel for in silico confirmation of RT-PCR primer specificities and complementary locations.

References

1. Wallace DC. Mitochondrial diseases in man and mouse. *Science.* 1999;283:1482–1488.
2. Doerner A, Pauschinger M, Badorff A, et al. Tissue-specific transcription pattern of the adenine nucleotide translocase isoforms in humans. *FEBS Lett.* 1997;414:258–262.
3. Stepien G, Torroni A, Chung AB, Hodge JA, Wallace DC. Differential expression of adenine nucleotide translocator isoforms in mammalian tissues and during muscle cell differentiation. *J Biol Chem.* 1992;267:14592–14597.
4. Graham BH, Waymire KG, Cottrell B, Trounce IA, MacGregor GR, Wallace DC. A mouse model for mitochondrial myopathy and cardiomyopathy resulting from a deficiency in the heart/muscle isoform of the adenine nucleotide translocator. *Nat Genet.* 1997; 16:226–234.
5. Esposito LA, Melov S, Panov A, Cottrell BA, Wallace DC. Mitochondrial disease in mouse results in increased oxidative stress. *Proc Natl Acad Sci U S A.* 1999;96:4820–4825.
6. Steinberg RH. Monitoring communications between photoreceptors and pigment epithelial cells: effects of "mild" systemic hypoxia: Friedenwald lecture. *Invest Ophthalmol Vis Sci.* 1987; 28:1888–1904.
7. Biousse V, Newman NJ. Neuro-ophthalmology of mitochondrial diseases. *Semin Neurol.* 2001;21:275–291.

8. Newman NJ. Mitochondrial disease and the eye. *Neuro-ophthalmol Syst Disease.* 1992;5:405–424.
9. Isashiki Y, Nakagawa M, Ohba N, et al. Retinal manifestations in mitochondrial diseases associated with mitochondrial DNA mutation. *Acta Ophthalmol Scand.* 1998;76:6–13.
10. Kaukonen J, Juselius JK, Tiranti V, et al. Role of adenine nucleotide translocator 1 in mtDNA maintenance. *Science.* 2000;289:782–785.
11. Chen XJ. Induction of an unregulated channel by mutations in adenine nucleotide translocase suggests an explanation for human ophthalmoplegia. *Hum Mol Genet.* 2002;11:1835–1843.
12. Agostino A, Valletta L, Chinnery PF, et al. Mutations of ANT1, Twinkle, and POLG1 in sporadic progressive external ophthalmoplegia (PEO). *Neurology.* 2003;60:1354–1356.
13. Virgilio R, Ronchi D, Hadjigeorgiou GM, et al. Novel Twinkle (PEO1) gene mutations in mendelian progressive external ophthalmoplegia. *J Neurol.* 2008;255:1384–1391.
14. Yin H, Stahl JS, Andrade FH, et al. Eliminating the Ant1 isoform produces a mouse with CPEO pathology but normal ocular motility. *Invest Ophthalmol Vis Sci.* 2005;46:4555–4562.
15. Ripps H, Peachey NS, Xu X, Nozell SE, Smith SB, Liou GI. The rhodopsin cycle is preserved in IRBP "knockout" mice despite abnormalities in retinal structure and function. *Vis Neurosci.* 2000; 17:97–105.
16. Bogazzi F, Raggi F, Ultimieri F, et al. Cardiac expression of adenine nucleotide translocase-1 in transgenic mice overexpressing bovine GH. *J Endocrinol.* 2007;194:521–527.
17. Flierl A, Chen Y, Coskun PE, Samulski RJ, Wallace DC. Adeno-associated virus-mediated gene transfer of the heart/muscle adenine nucleotide translocator (ANT) in mouse. *Gene Ther.* 2005;12: 570–578.
18. Andrews RM, Griffiths PG, Johnson MA, Turnbull DM. Histochemical localisation of mitochondrial enzyme activity in human optic nerve and retina. *Br J Ophthalmol.* 1999;83:231–235.
19. Hood DC, Birch DG. The A-wave of the human electroretinogram and rod receptor function. *Invest Ophthalmol Vis Sci.* 1990;31: 2070–2081.
20. Lamb TD, Pugh EN Jr. A quantitative account of the activation steps involved in phototransduction in amphibian photoreceptors. *J Physiol.* 1992;449:719–758.
21. Kofuji P, Ceelen P, Zahs KR, Surbeck LW, Lester HA, Newman EA. Genetic inactivation of an inwardly rectifying potassium channel (Kir4.1 subunit) in mice: phenotypic impact in retina. *J Neurosci.* 2000;20:5733–5740.
22. Robson JG, Frishman LJ. Dissecting the dark-adapted electroretinogram. *Doc Ophthalmol.* 1999;95:187–215.
23. Wachtmeister L. Further studies of the chemical sensitivity of the oscillatory potentials of the electroretinogram (ERG), II: glutamate-aspartate-and dopamine antagonists. *Acta Ophthalmol (Copenh).* 1981;59:247–258.
24. Wachtmeister L, Dowling JE. The oscillatory potentials of the mudpuppy retina. *Invest Ophthalmol Vis Sci.* 1978;17:1176–1188.
25. Li C, Cheng M, Yang H, Peachey NS, Naash MI. Age-related changes in the mouse outer retina. *Optom Vis Sci.* 2001;78:425–430.
26. Pardue MT, McCall MA, LaVail MM, Gregg RG, Peachey NS. A naturally occurring mouse model of X-linked congenital stationary night blindness. *Invest Ophthalmol Vis Sci.* 1998;39:2443–2449.
27. Cheng T, Peachey NS, Li S, Goto Y, Cao Y, Naash MI. The effect of peripherin/rds haploinsufficiency on rod and cone photoreceptors. *J Neurosci.* 1997;17:8118–8128.
28. Burmeister M, Novak J, Liang MY, et al. Ocular retardation mouse caused by Chx10 homeobox null allele: impaired retinal progenitor proliferation and bipolar cell differentiation. *Nat Genet.* 1996; 12:376–384.
29. Milam AH, Dacey DM, Dizhoor AM. Recoverin immunoreactivity in mammalian cone bipolar cells. *Vis Neurosci.* 1993;10:1–12.
30. Robson JG, Frishman LJ. Response linearity and kinetics of the cat retina: the bipolar cell component of the dark-adapted electroretinogram. *Vis Neurosci.* 1995;12:837–850.
31. Sieving PA, Murayama K, Naarendorp F. Push-pull model of the primate photopic electroretinogram: a role for hyperpolarizing neurons in shaping the b-wave. *Vis Neurosci.* 1994;11:519–532.
32. Gouras P, Eggers HM, MacKay CJ. Cone dystrophy, nyctalopia, and supernormal rod responses: a new retinal degeneration. *Arch Ophthalmol.* 1983;101:718–724.
33. Yagasaki K, Miyake Y, Litao RE, Ichikawa K. Two cases of retinal degeneration with an unusual form of electroretinogram. *Doc Ophthalmol.* 1986;63:73–82.
34. Alexander KR, Fishman GA. Supernormal scotopic ERG in cone dystrophy. *Br J Ophthalmol.* 1984;68:69–78.
35. Heckenlively JR, Tanji T, Logani S. Retrospective study of hyperabnormal (supranormal) electroretinographic responses in 104 patients. *Trans Am Ophthalmol Soc.* 1994;92:217–231, discussion 231–233.
36. Buck CR, Jurynec MJ, Gupta DK, et al. Increased adenine nucleotide translocator 1 in reactive astrocytes facilitates glutamate transport. *Exp Neurol.* 2003;181:149–158.
37. Newman EA. New roles for astrocytes: regulation of synaptic transmission. *Trends Neurosci.* 2003;26:536–542.
38. Ettaiche M, Heurteaux C, Blondeau N, Borsotto M, Tinel N, Lazdunski M. ATP-sensitive potassium channels (K(ATP)) in retina: a key role for delayed ischemic tolerance. *Brain Res.* 2001;890:118–129.
39. Linsenmeier RA. Effects of light and darkness on oxygen distribution and consumption in the cat retina. *J Gen Physiol.* 1986;88: 521–542.
40. Wolbarsht ML, George GS, Shearin WA Jr, Kylstra JA, Landers MB 3rd. Retinopathy of prematurity: a new look at an old disease. *Ophthalmic Surg.* 1983;14:919–924.
41. Cooper LL, Hansen RM, Darras BT, et al. Rod photoreceptor function in children with mitochondrial disorders. *Arch Ophthalmol.* 2002;120:1055–1062.